MAGNETIC RESONANCE NEUROGRAPHY AND DIFFUSION TENSOR IMAGING: ORIGINS, HISTORY, AND CLINICAL IMPACT OF THE FIRST 50 000 CASES WITH AN ASSESSMENT OF EFFICACY AND UTILITY IN A PROSPECTIVE 5000-PATIENT STUDY GROUP

Aaron Filler, M.D., Ph.D.

Institute for Nerve Medicine,
Santa Monica, California

Reprint requests:
Aaron G. Filler, M.D., Ph.D.,
Institute for Nerve Medicine,
2716 Ocean Park Boulevard #3082,
Santa Monica, CA 90405.
Email: afiller@nervemed.com

Received, April 30, 2008.
Accepted, April 21, 2009.

OBJECTIVE: Methods were invented that made it possible to image peripheral nerves in the body and to image neural tracts in the brain. The history, physical basis, and dyadic tensor concept underlying the methods are reviewed. Over a 15-year period, these techniques—magnetic resonance neurography (MRN) and diffusion tensor imaging—were deployed in the clinical and research community in more than 2500 published research reports and applied to approximately 50 000 patients. Within this group, approximately 5000 patients having MRN were carefully tracked on a prospective basis.

METHODS: A uniform Neurography imaging methodology was applied in the study group, and all images were reviewed and registered by referral source, clinical indication, efficacy of imaging, and quality. Various classes of image findings were identified and subjected to a variety of small targeted prospective outcome studies. Those findings demonstrated to be clinically significant were then tracked in the larger clinical volume data set.

RESULTS: MRN demonstrates mechanical distortion of nerves, hyperintensity consistent with nerve irritation, nerve swelling, discontinuity, relations of nerves to masses, and image features revealing distortion of nerves at entrapment points. These findings are often clinically relevant and warrant full consideration in the diagnostic process. They result in specific pathological diagnoses that are comparable to electrodiagnostic testing in clinical efficacy. A review of clinical outcome studies with diffusion tensor imaging also shows convincing utility.

CONCLUSION: MRN and diffusion tensor imaging neural tract imaging have been validated as indispensable clinical diagnostic methods that provide reliable anatomic pathological information. There is no alternative diagnostic method in many situations. With the elapsing of 15 years, tens of thousands of imaging studies, and thousands of publications, these methods should no longer be considered experimental.

KEY WORDS: Brachial plexus, Brain, Diffusion tensor imaging, Magnetic resonance imaging, Nerve, Piriformis, Thoracic outlet

Neurosurgery 65:A29–A43, 2009 DOI: 10.1227/01.NEU.0000351279.78110.00 www.neurosurgery-online.com

The discovery of a series of magnetic resonance pulse sequence strategies for tissue-specific imaging of nerve and nerve tracts in 1991 and 1992 opened a new diagnostic world in which a wide variety of pathological conditions involving nerves and neural tracts can be visualized directly (5, 7, 22, 29, 32, 38, 39, 59); these techniques are grouped under the terms *magnetic resonance neurography* (MRN) for peripheral nerves and *diffusion tensor imaging* (DTI) or *tractography* for the central nervous system (CNS). Many specialists in these 2 fields are not aware that they have a common origin in a shared set of fundamental imaging strategies and algorithms that grew out of a unitary development project.

ABBREVIATIONS: ADC, apparent diffusion coefficient; **CNS**, central nervous system; **DTI**, diffusion tensor imaging; **DWI**, diffusion-weighted imaging; **FA**, fractional anisotropy; **MRI**, magnetic resonance imaging; **MRN**, magnetic resonance neurography; **3-D**, 3-dimensional

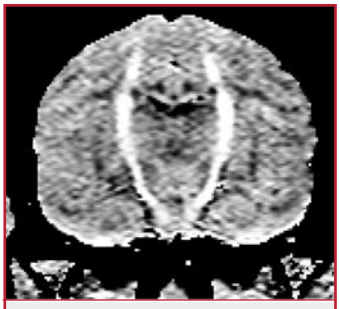

FIGURE 1. *First diffusion tractographic imaging case. This image is primarily the work of Todd Richards and shows the use of spatial diffusion information to highlight a neural tract curving through brain. This is the brain of a long-tailed macaque monkey (*Macaca fascicularis*) imaged as part of an effort to improve the sensitivity of magnetic resonance imaging for the early detection of encephalomyelitis. (From Filler AG, Tsuruda JS, Richards TL, Howe FA, inventors; University of Washington, assignee. Images, apparatus, algorithms and methods. UK patent GB920016383. July 31, 1992 [29]; and Filler AG, Tsuruda JS, Richards TL, Howe FA, inventors; University of Washington, assignee. Image neurography and diffusion anisotropy imaging. US patent 5,560,360. March 8, 1993 [30]).*

The first tractographic image using multidimensional directional information to show curved neural tracts traversing the brain (Fig. 1) and the first neurography images were submitted in a series of United Kingdom patent descriptions by Filler et al. (24, 29) between March and July of 1992 and were published by the World Intellectual Property Organization in 1993 (26, 30). Related images were published in the proceedings of the Society for Magnetic Resonance in Medicine annual meeting in Berlin in August 1992 (39, 59).

Before these developments in 1992, it had been generally assumed among radiologists that the peripheral nerves simply could not be imaged reliably. The potential to use diffusion magnetic resonance imaging (MRI) to tract trace through the brain was also not really anticipated in the clinical community. The strategy of using diffusion-based MRI sequences to help produce linear neural images was first discussed by Filler et al. in 1991 (32) and emerged as a workable technique through discoveries by Filler, Howe, and Richards (in London and Seattle) in late 1991 and by LeBihan and Basser (in Bethesda) in early 1992.

As a historical note, it is worth mentioning that the original work on DTI and Neurography in London was funded by the Neuroscience Research Foundation of Atkinson Morley's Hospital—the site where Hounsfield built the first experimental computed tomographic scanner in 1971 and also the site of the first clinical computed tomographic scan in 1973 (3, 37).

Treatment of each image voxel as a mathematical entity for vector and tensor math analysis represented a fundamental rethinking of neurological imaging data. This constituted a very significant transformation of the legacy of cross-sectional imaging from computed tomographic scanning—with its conceptual origins in X-ray beams and film exposures.

Vector and tensor representation of the internal structure of voxel image data also represented a shift in the conceptual basis of MRI from "slab"-based neuroanatomy into the realm of tract tracing that had dominated neuroanatomic research in the 1970s and 1980s. Interest in tract tracing for evolutionary studies of uniquely human neuroanatomic structures in the brain related to speech (12, 13) and in the periphery related to the lumbar reorganization in hominoids (15, 17–19, 22, 33, 49) provided the original impetus for development of imageable tractographic methods for the CNS and nerves (16, 31).

Previously, the methodology of MRI had been focused on identifying methods to assign contrasting image intensities to various voxels (3-dimensional [3-D] pixels) in an MRI slice. This was accomplished by a wide array of pulse sequences that manipulated aspects of the T1 and T2 relaxation time of protons. Positional information for the voxels was obtained by using magnetic gradients to assign unique magnetic field strengths to each location in the volume to be imaged and then using Fourier transforms to extract signal strength data from each voxel at various echo times after a simple or complex radiofrequency pulse. Diffusion nuclear magnetic resonance per se had also known for decades; it acted as yet another source for obtaining contrast on the voxels by assessing relaxation rates (signal decays) that related to the degree to which nerve fibers tended to have water diffuse anisotropically (in a primary direction) rather than isotropically (in all directions) (52, 53). This is the basis for the diffusion-weighted imaging (DWI) that has been used to detect strokes for many years (43, 51, 56).

In magnetic resonance angiography, we typically produce a series of image slices in which blood vessel voxels are bright and then reconstruct the vessel tree from a stack of slices with vessels shown prominently in each cross section. DTI works very differently. The critical insight was a modification in the fundamental data acquisition process of the MRI scanning system so that each voxel would yield not only image intensity data but also directional data showing the tensor (3-D complex vector) direction in 3-D space.

Each voxel could be represented by a small arrow pointed in the direction of the principal nerve orientation in that volume. Instead of producing a cross section with dots, we produce an array of directional arrows along neural tracts, and these can be strung together by various standard 3-D graphics techniques to produce linear images of nerve tracts. In addition, pulse sequence modifications could be applied that made these data discoverable in the peripheral nerve as well. The resulting neurograms then served as a model for discovering additional non-diffusion tractographic methods for peripheral nerves.

By 1993, there were several major publications in these fields (25, 30, 36). In the subsequent 15 years, more than 100 academic publications have reported on various aspects of this new imaging modality in peripheral nerves, including several large-scale formal outcome assessment trials (23, 41, 42). Nonetheless, most textbooks of radiology or neuroradiology do not devote any pages to nerve imaging (4), as if nerves were not a clinically significant part of the body. Most practicing physicians still do not realize that high-quality diagnostically efficacious nerve imaging is available.

More than 2000 studies that explore DTI tractography in the CNS have been published (55), with most of these appearing in the past 3 years. The clinical impact of DTI is still difficult to predict. However, it encodes a great deal of information that is usually discarded in the course of CNS imaging. Therefore, it has shown great promise for detecting subtle derangements of

brain architecture that are difficult to recognize with cross-sectional imaging.

Formal outcome studies on the use of DTI for evaluation of traumatic brain injury (60), for predicting outcome after intracerebral hemorrhage (63), and for surgical guidance to optimize glioma resection (62) have appeared along with numerous preliminary studies for a wide variety of clinical uses in neuroscience, such as in the evaluation of dementia in Alzheimer's disease (10) and in identifying subtle lesions involved in the etiology of epilepsy (14). Recent diffusion image presentation algorithms have also been used to further advance earlier work on the use of DTI for peripheral nerves (38, 46, 61).

In the smaller but more clinical peripheral nerve imaging arena, MRN has proven to be more efficacious than electrodiagnostic studies for identifying nerve compressions that will improve with surgical treatment. This efficacy is seen both in diagnoses that are typically evaluated by electrodiagnostic studies such as carpal tunnel syndrome (41, 42) and in diagnoses in which electrodiagnostic studies have proven difficult such as piriformis syndrome and related sciatic nerve entrapments (20, 23).

The utility of MRN has now been established in the evaluation of entrapment syndromes (1, 2, 23, 27, 50), in the evaluation of nerve injury/repair (11), in nerve tumor assessment (8, 34, 35), and in the setting of neuritis and a variety of neuropathies (28). It is also effective for evaluating nerve disorders affecting young pediatric patients such as obstetrical brachial plexus palsy.

Over the 15 years since MRN was initially brought into clinical use, approximately 25 000 peripheral nerve imaging studies have been conducted. DTI in conjunction with brain MRI scans has been performed in tens of thousands of patients, mostly in the past 2 years. This report assesses the use and diagnostic range for MRN in a prospective group of more than 5000 patients for whom standardized protocols were applied, research consent obtained, and clinical data collected and organized.

For both T2 MRN and DTI, the clinical results can be used to help verify hypotheses about the physical basis of the underlying biophysical phenomena that result in the observed image effects in both normal and pathological situations. In addition, by identifying the most effective parameters to optimize, the clinical results can best identify the way forward for future developments.

PATIENTS AND METHODS

All patients had a physical examination to identify specific suspect nerve pathological conditions. Images were ordered through St. George's Hospital Medical School (1992–1996); University of Washington Department of Radiology (1993–1995); University of California, Los Angeles or OliveView/ University of California, Los Angeles Department of Radiology (1996–2001); or the Neurography Institute (2000–2007). Image protocols included matched T1 (anatomic) and neurographic image pulse sequences in multiple planes including at least one "nerve perpendicular" plane for fascicle assessment. Echo times were greater than 40 milliseconds (usually 70–100 milliseconds) for all MRN studies to assure that no magic angle effects could occur (8). Referral biases toward these specialty centers because of their widely recognized expertise in this area was an unavoidable aspect of the data.

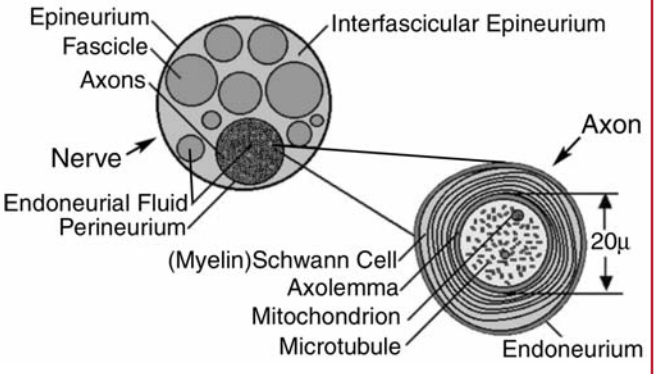

FIGURE 2. *Nerve water compartments. Magnetic resonance pulse sequences can be optimized to detect a water signal arising in one of several compartments. Important nerve water components with unique characteristics for magnetic resonance imaging include the endoneurial fluid, axoplasmic water, organelle water, and myelin-associated water.*

RESULTS

T2-based MRN

Physical Basis

The clinical pathological data in T2-based MRN seem to derive from alterations in endoneurial fluid content in nerves. This fluid seems to be the sole candidate for the class of water to which the image parameters should apply. It is a low-protein fluid (long T2), confined to the endoneurium of nerve fascicles (Fig. 2), that physiologically participates in a bulk proximal to distal flow (54, 57, 58). Compressions or irritative processes seem to be capable of increasing the amount of this fluid relative to the other cellular components of the fascicle in a variety of pathological conditions (40).

Usage by Type of Pathological Condition

The dominant class of pathological conditions for which MRN studies were ordered in this group were for nerve entrapment. Usage in tumors (Figs. 3 and 4), trauma (Fig. 5), and neuropathy represented only a very small percentage of the studies. However, this usage also reflects the relative incidence of these conditions. Nerve entrapment/degenerative problems such as carpal tunnel syndrome, piriformis syndrome, thoracic outlet syndrome, and radicular spinal syndromes are far more prevalent. When correction for incidence of the major classes of disorders is considered, the usage pattern seems to be similar for degenerative/pain/entrapment, neoplastic, and traumatic nerve pathological conditions. Our study participants represented approximately 0.01% of the total incidence for the time period for these types of cases. Usage for the evaluation of neuropathy is very low.

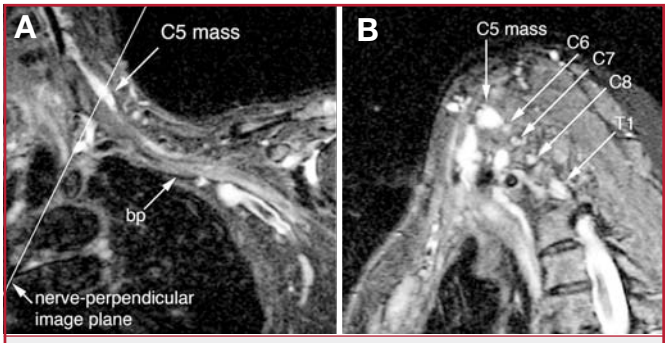

FIGURE 3. *Relations of a small C5 mass to brachial plexus (bp) elements. In many patients, by collecting images in planes that are perpendicular to the main longitudinal axis of the nerve elements of interest, it is possible to obtain extremely specific information about the location of a mass within the brachial plexus.* **A**, *multiplanar reformat oriented parallel to the main longitudinal orientation of the brachial plexus.* **B**, *oblique acquisition perpendicular to the orientation of the main longitudinal direction of the brachial plexus.*

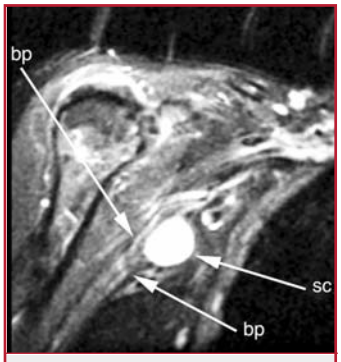

FIGURE 4. *Relations of brachial plexus (bp) elements to an axillary mass. Although a schwannoma (sc) can be detected by various techniques, it is extremely valuable for the surgeon to have a method of determining the position of the nerve elements relative to the position of the mass.*

Usage by Body Region/Nerve

Use of MRN is heavily concentrated in the evaluation of large proximal nerves that are difficult to assess accurately by routine electrodiagnostic techniques and physical examination. Studies of the lumbosacral plexus, proximal sciatic nerve, and other pelvic nerves (ilioinguinal, pudendal, femoral, and obturator) constituted approximately 42% of cases. Brachial plexus imaging accounted for an additional 18% of cases and lumbar spinal nerve studies accounted for 5%. The remaining 35% were studies of knee/peroneal nerve, elbow/ulnar nerve, wrist/median nerve, ankle/tibial nerve, upper neck/occipital nerves, and thigh/distal sciatic, calf, foot, upper arm, abdominal wall, face, intercostal spaces, and various individual study types.

Usage by Practitioner Category

Most MRN studies were ordered by neurosurgeons (43%), and this ordering seemed to represent a combined influence of diagnostics and surgical planning. Surgical planning as a reason for ordering was inferred when the study was ordered by a surgeon and the diagnosis was already established. Neurologists ordered an additional 21% of the studies, whereas pain specialists (12%), physiatrists (8%), orthopedic surgeons (6%), and various others ordered the remaining studies. Only a very small number were ordered for pediatric patients, and these generally were not ordered by pediatricians.

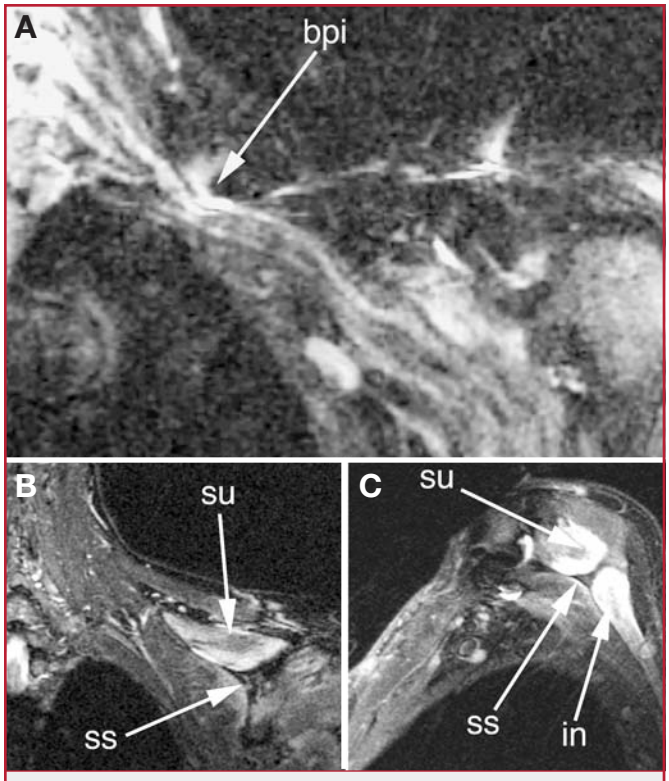

FIGURE 5. *Upper trunk brachial plexus injury (bpi) with denervation of C5 muscles.* **A**, *apparent discontinuity of the C5 component of the upper trunk. The C6 component is swollen upstream of the injury and sharply narrowed and hyperintense. Coronal view (***B***) and nerve perpendicular view (***C***) showing severe denervation changes in supraspinatus (su) and infraspinatus (in) muscles. ss, scapular spine.*

Diagnostic Efficacy and Ordering

MRN had a high diagnostic efficacy. More than 96% of studies resulted in either specific findings involving the nerve of interest or in a definitive statement that the nerve or nerves in question were entirely normal in appearance. The remaining 4% of studies were nondiagnostic because of movement, artifact from implants, body habitus or pain limiting appropriate positioning in the scanner, or ordering errors. Ordering errors arose because many practitioners were not experienced in ordering nerve imaging. For example, a neurologist or neurosurgeon (or staff member) seeking to evaluate sciatica due to piriformis syndrome would order a lumbar MRN instead of the necessary pelvic MRN because of the habit of using lumbar MRI for sciatica.

Contrast Agent Use

Intravenous gadolinium contrast material was used in approximately 0.4% of cases. When tumor was part of an initial

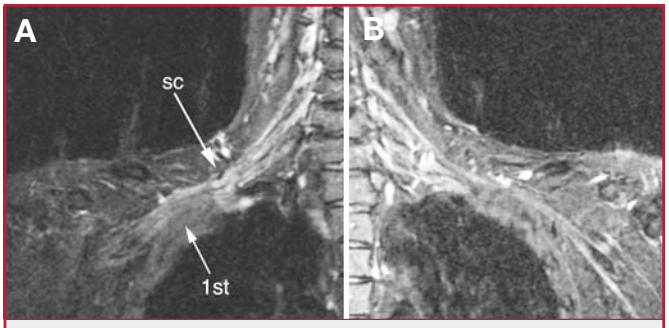

FIGURE 6. *Right and left side comparison of a patient suffering from right-sided thoracic outlet syndrome. The image demonstrates several types of abnormalities detectable by magnetic resonance neurography relative to the normal side. There is increased caliber and image intensity of nerve elements on the left and 2 sites of impingement. A sharp focal downward distortion at the lateral border of the scalene triangle (sc) and then a gently sloped upward distortion over the first rib (1st).*

differential diagnosis but not proven, contrast material was not used. Only patients with known tumors underwent intravenous contrast studies.

Follow-up Imaging Studies

Approximately 1% of the studies were part of a repetitive set. These were generally done in patients who had diagnostic MRN and were then referred for repeat imaging when symptoms recurred after treatment, when an extended time elapsed between initial imaging and treatment, when recurrent tumor was suspected, or when new symptoms arose in the same body region. Generally, the use of repetitive imaging was lower that what has been reported for lumbar or cervical MRI.

Geographic Distribution

The highest usage of MRN was in Southern California, accounting for approximately 82% of patients imaged. Usage was lower in other regions with the only other significant concentration being in Northern California and the remainder coming from nearly all states in the United States, England, Spain, France, Japan, Mexico, and China.

Classes of Image Findings

Image findings in MRN studies include the presence of regions of nerve hyperintensity, distortions of normal nerve course, abnormal contours, and alterations of nerve caliber (Figs. 6 and 7), any of which can be classed by the degree or severity of the abnormality. These findings seem most reliable for the larger named nerves (>3 mm in diameter), although there is no technical limit on the imageable size of a nerve. In trauma, assessments of nerve continuity (Fig. 5) and/or location of severed nerve endings are feasible, although edema at a site of injury limits the utility of MRN in acute injury settings, but this becomes less of an issue after the elapse of 2 to 4 weeks. In chronic trauma or late evaluation of the effects of trauma, the development of fibrosis does not hinder nerve imaging because most classes of fibrosis have very different image characteristics than nerve: there is no long T2 low-protein water component to deal with.

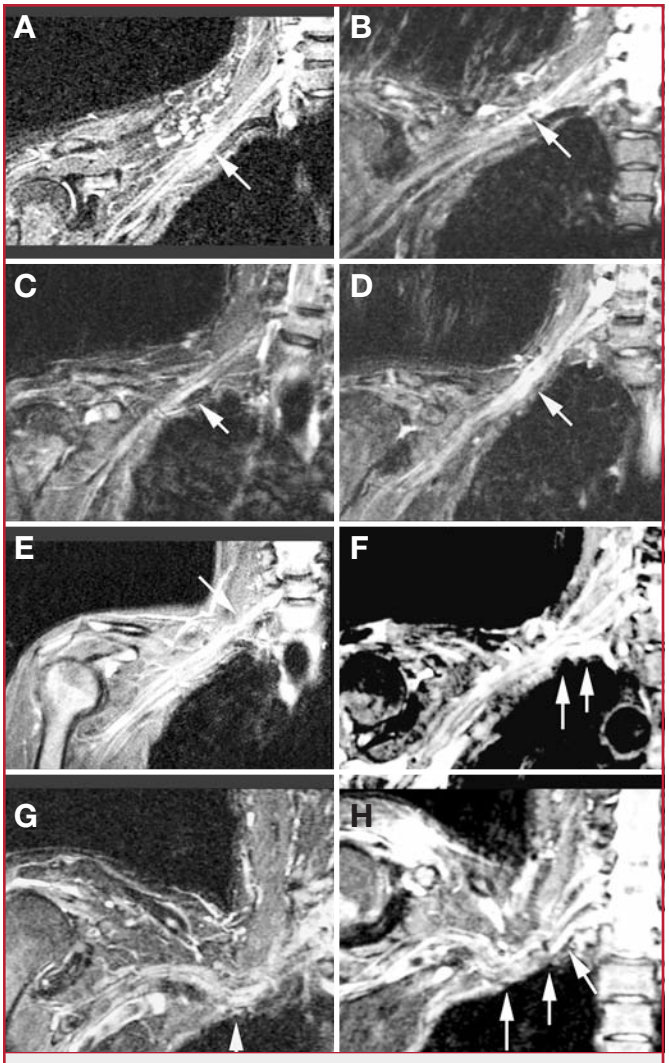

FIGURE 7. *Varying degrees of severity of brachial plexus entrapment in thoracic outlet syndromes.* **A**, *linear plexus with short segment of mild hyperintensity consistent with nerve irritative changes near the later border of the scalene triangle.* **B**, *evidence of more restrictive fibrosis associated with narrowing and brightening of plexus elements near the scalene border (note linear plexus despite elevated shoulder).* **C**, *short segment of marked hyperintensity with slight swelling.* **D**, *severe multiple element abnormality with narrowed and swollen segments and marked hyperintensity.* **E**, *linear normal plexus with isolated focal impingement of C5 spinal nerve, just proximal to the scalene triangle.* **F**, *fibrous band causing sharp downward distortion of the mid and lower trunk proximal to the scalene triangle, with a second sharp upward distortion of the lower trunk near scalene insertion at the first rib.* **G**, *moderate restrictive impingement of plexus at the scalene triangle causing generalized distortion of the course of the plexus with a short segment of focal hyperintensity.* **H**, *patient presenting with severe pain, numbness, and weakness from progressive thoracic outlet syndrome: multiple points of sharp nerve course distortion with edema and hyperintensity affecting multiple brachial plexus elements.*

Conspicuity and Reconstructions

One important aspect of MRN is to use MRI pulse sequences and acquisition strategies that tend to make nerve image intensity brighter than that of immediately surrounding tissues. When this is achieved, it greatly aids the process of generating 3-D projection images as well as multiplanar reformatted images. This process often helps in the recognition of the overall nerve course and of variations in the types of other image findings along the length of a nerve. Among the 5000 patients evaluated, 3-D analysis could be used in more than 99%. Findings in the 3-D reports revealed additional information not recognized in 2-dimensional analysis in 28% of patients. The greatest amount of additional diagnostic information in these analyses occurred in the brachial plexus studies. Because of the significant incremental amount of clinical information provided by this type of analysis and the susceptibility of most studies, these were considered essential aspects of the diagnostic interpretation process in this group.

Multiplanar reformat and maximum intensity projection reconstructions were also important in limiting artifactual variations in nerve image intensity that can occur from partial volume averaging; this means that when a given sampled voxel is partially filled with nerve and partially filled with an adjacent low-intensity tissue, the resulting pixel on the image will appear to show low-intensity nerve. Reconstruction techniques such as multiplanar reformats in linear planes allow the reading clinicians to readily assess this sort of issue. Curved reformats made along a "nerve course plane" drawn along the main nerve axis by a technologist or radiologist reduce the accuracy of the spatial information but provide for optimal reduction of image intensity averaging effects.

Image Findings in Brachial Plexus Studies

MRN proved effective for identifying the presence of a variety of types of abnormalities in brachial plexus studies. These include distortions of the course of the proximal elements at the scalene triangle (Figs. 6 and 7, A–D), fibrous band entrapments affecting C8 and T1 spinal nerve and the lower trunk of the brachial plexus (Fig. 7F), gross distortions of the midplexus (Figs. 7, G and H), hyperintensity consistent with nerve irritation at the level of the first rib (Fig. 6), and distal plexus hyperintensity.

In most peripheral nerve studies it has proven useful for identifying areas of hyperintensity consistent with nerve irritation by a comparison of results from following serial nerve cross sections oriented to be perpendicular to the principal long axis of nerves to images taken to be more or less parallel to the long axis. In nerve perpendicular images, the fascicle pattern can generally be observed. This will demonstrate expansion of the fascicle compartment at the expense of the interfascicular compartment at areas of focal hyperintensity. The nerve parallel images can provide a linear overview. In general, effective interpretation of nerve parallel images depends on the ability of the MRN imaging sequence to make the nerve brighter than surrounding tissues. In this fashion the nerve image plane can be adjusted by multiplanar reformatting or the nerve can be assembled by maximum intensity projection. If this is not done, partial volume effects at the edges of nerves can lead to the artifactual appearance of variation of image intensity within an image. In the brachial plexus, multiplanar reformatting is usually sufficient to generate a series of images that can reliably confirm the existence of a focal change in nerve image intensity. This is aided by positioning the patient in the scanner in a way that tends to straighten the plexus. When a change in the fascicle pattern shows increased intensity in the nerve perpendicular views that matches a change seen in nerve parallel views, there can be a very high level of confidence about the clinical reality of nerve edema at the location that appears abnormal in the image.

MRN in the Pelvis

The use of MRN has revolutionized neurological diagnosis in the pelvis (20, 21, 23). Although sciatic pathological conditions have been an important part of the progress, the ability of MRN to track other nerve elements in the pelvis has contributed greatly to resolving what had been a troublesome "black box."

Patients with face, neck, arm, and hand conditions tend to be very effective in identifying the location of pain, numbness, and dysfunction. The physical examination is straightforward and well understood by many clinicians. Electrodiagnostic studies are readily applied. In the pelvis, the situation is quite different. Although the sciatic nerve in the leg poses accessibility similar to what the clinician experiences in the upper body, there has been great difficulty in applying physical examination and imaging and electrodiagnostic studies in the pelvis. Furthermore, patients often have great difficulty explaining the location of pains. It is common for low buttock pain to be described as "back pain," whereas patients readily distinguish between shoulder and neck pain. "Groin" pain could refer to problems involving the femoral nerve, ilioinguinal nerve, genitofemoral nerve, pudendal nerve, obturator nerve, or nerve to the obturator internus, among others.

The ability to reliably locate all of these nerve elements in MRN images greatly aids in physical examination. The ability of open magnetic resonance-guided injections to distinguish the superior gluteal nerve, inferior gluteal nerve, posterior femoral cutaneous nerve, cluneal nerve (superior, middle, and inferior), nerve to the obturator internus, and nerve to the quadratus femoris has also supplemented the role of MRN for identifying pathological conditions in these nerves. Clarification of the nerve course anatomy has also greatly enhanced the efficacy of a physical examination and elucidated the meaning of a variety of new types of physical examination maneuvers.

With regard to lower extremity radiculopathy, MRN has made it convenient to determine distinctions by imaging that help locate impingements in spinal foramina, at the distal foramen, at the lateral marginal osteophytes several centimeters distal to the foramen (Fig. 8), in the lumbosacral plexus, on the medial aspect of the piriformis muscle (Fig. 9), in association with division of the nerve by the piriformis muscle (Fig. 10), at the ischial margin, at the tendon of the obturator internus, at the distal ischial tunnel on the lateral aspect of the ischial tuberosity, and at various locations in the thigh. Because MRN is a very sensitive test, a completely negative MRN result (Fig.

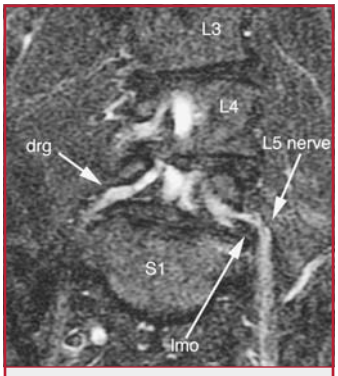

FIGURE 8. *Extraforaminal impingement of descending L5 spinal nerve by lateral marginal osteophyte distal to the foramen. drg, dorsal root ganglion, lmo, lateral marginal osteophyte.*

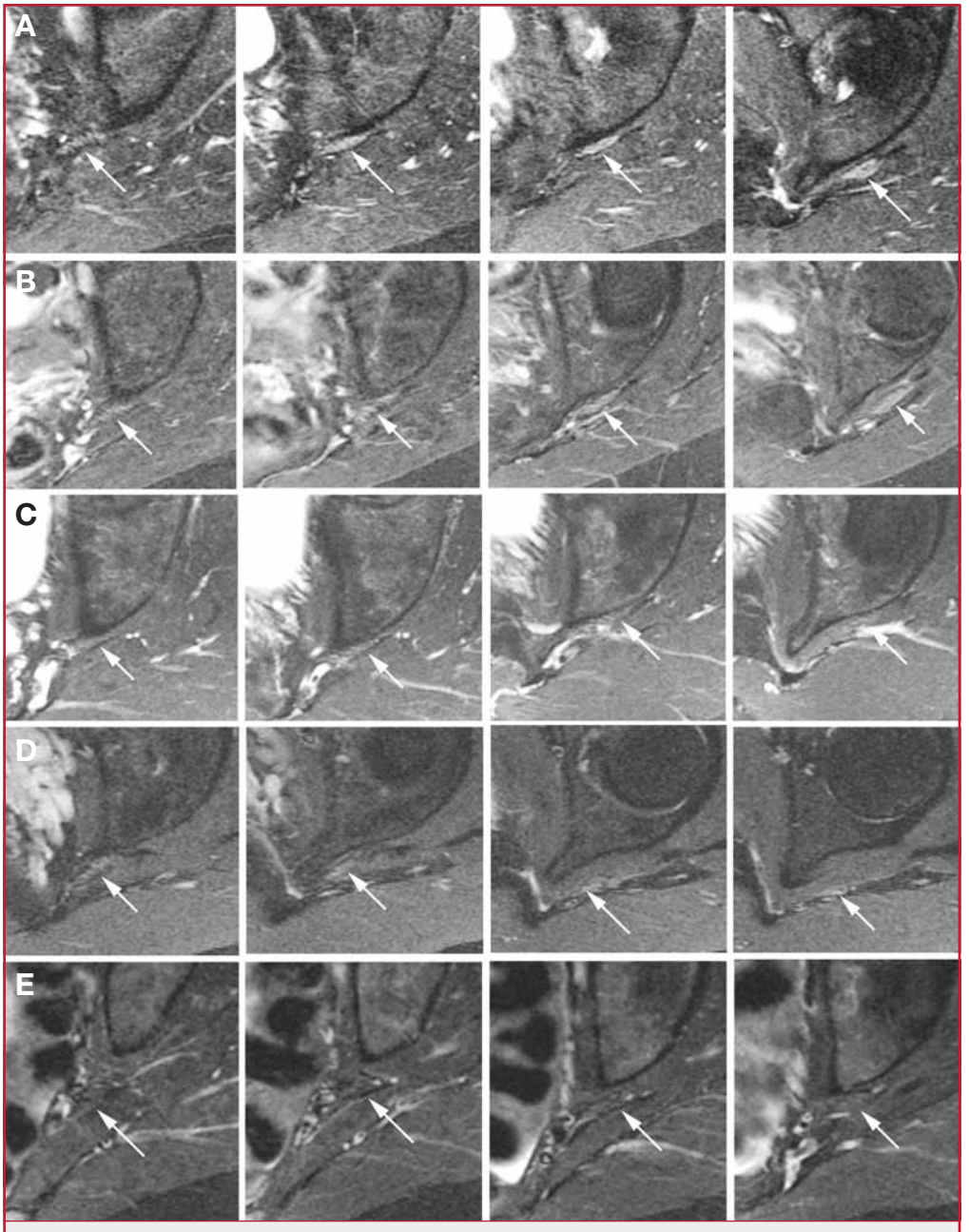

FIGURE 9. *Comparison of sciatic nerve appearance at the sciatic notch in patients with hyperintensity and in normal patients.* **A** *and* **B**, *hyperintensity in the sciatic nerve in a series of images as the nerve exits the sciatic notch and descends below the level of the piriformis tendon.* **C**, **D**, *and* **E**, *sciatic nerve is nearly isointense with surrounding muscle tissue. Arrow indicates sciatic nerve in all images.*

9) is often very useful, just as a completely normal lumbar MRI scan can be. In both cases, the definitively negative study results can substantively change the direction of further diagnostic efforts.

Reliable identification of anatomic variants of the sciatic nerve now plays a critical role in improving the safety of operations for the release of pelvic sciatic nerve entrapment. Isolated section of a single piriformis segment in patients with a split nerve passing through a split muscle can cause nerve compromise after surgery if this condition is not detected in advance (Fig. 11). Identification of the presence or absence of pudendal nerve hyperintensity consistent with nerve irritation in the Alcock canal (Fig. 12) along the medial aspect of the obturator internus muscle or at the rectal branch of the pudendal nerve proximal to its entrance to the Alcock canal (Fig. 13) has also been quite useful clinically (21).

Imaging of the complete course of the L4 spinal nerve as it progresses into the femoral nerve has made it possible to search for abnormalities along the intra-abdominal and intrapelvic course that were previously almost impossible to diagnose. Identification of abnormalities along the ilioinguinal and genitofemoral nerves is similarly greatly aided by MRN.

Nerve Imaging for Distal Entrapments

Patients with distal entrapments including less common problems such as posterior interosseous nerve entrapment of the distal radial nerve as well as common issues such as peroneal nerve entrapment at or above the fibular head, tarsal tunnel syndrome, cubital tunnel syndrome, and carpal tunnel syn-

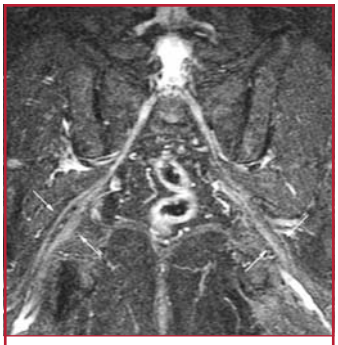

FIGURE 10. *Bilateral split sciatic nerve at the piriformis muscle in patient with bilateral piriformis syndrome. Among the most important aspects of preoperative planning in management of sciatic nerve entrapments in the pelvis is the identification of patients with a split sciatic nerve partly passing through the piriformis muscle. This image demonstrated the S1 spinal roots, spinal nerves, lumbosacral plexus, and split peroneal and tibial components of the sciatic nerve (arrows) as they are deviated by segments of the piriformis muscle bilaterally.*

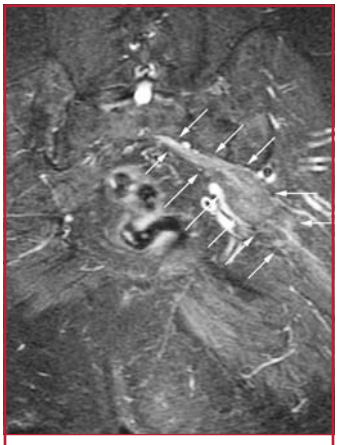

FIGURE 11. *Severe focal compression of the sciatic nerve at the sciatic notch. The nerve is flattened, hyperintense, and expanded to more than twice its normal diameter. This is a postoperative result that occurred when only one of the 2 bipartite elements of the piriformis muscle was released in a patient with split nerve and split muscle. Differential retraction of the cut piriformis segment relative to the intact segment caused a severe mechanical impingement syndrome.*

drome benefit from MRN imaging when a physical examination or electrodiagnostic studies show that locations other than the most routine sites may be involved. For instance, median nerve entrapment in the distal forearm can lead to failure of treatment if only the flexor retinaculum is addressed. Ulnar entrapment in the Guyon canal and proximal peroneal nerve entrapments along the tendon of the biceps femoris just distal to the sciatic bifurcation are other specialized issues that can be investigated best by imaging. Electrodiagnostic studies can be misleading if they are done with the assumption that abnormalities in certain regions (e.g., the median nerve in the distal forearm) will always be at the flexor retinaculum, particularly if uncomfortable and time-consuming "inching" studies are not done.

Clinical Outcomes nd MRN

The evidence for clinical utility for MRN has been evaluated with 2 different types of outcome studies. First, it has been compared with electrodiagnostic studies in the well-defined environment of assessing median nerve compressions at the wrist (41, 42). In this setting, in the evaluation of 120 patients, MRN has proven to be as effective or slightly better than electrodiagnostic studies for predicting which patients will have good surgical outcome from carpal tunnel decompression. Second, a different paradigm has been applied using class A study methodology for evaluating the utility of MRN for positively affecting patient outcomes in proximal sciatic entrapment, a condition for which there is no gold standard method (23, 44, 45). In this study evaluating 239 patients, use of MRN resulted in a strongly significant improvement in success for treating patients with sciatica who had either negative diagnostic study results or in whom treatment failed when managed by information from standard diagnostic studies alone. In these studies, image interpretation was performed by neuroradiologists blinded to outcome results.

FIGURE 12. *Pudendal nerve entrapment between the ischial spine and the Alcock canal. In patients with unilateral pudendal entrapment in the Alcock canal, it is typical to see asymmetric swelling and hyperintensity affecting the pudendal neurovascular bundle. Note increased caliber and hyperintensity at the left pudendal nerve indicated by the left arrow. (From Filler AG: Diagnosis and management of pudendal nerve entrapment syndromes: Impact of MR neurography and open MR-guided injections. **Neurosurg Q** 18:1–6, 2008 [21]).*

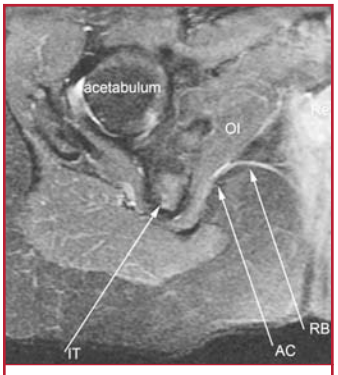

FIGURE 13. *Distal pudendal nerve neurographic image anatomy. The pudendal nerve in the Alcock canal (AC) runs along the medial aspect of the obturator internus muscle (OI) medial to the ischial tuberosity (IT). The rectal branch of the nerve (RB) is well seen in most imaging studies. Re, rectum. (From Filler AG: Diagnosis and management of pudendal nerve entrapment syndromes: Impact of MR neurography and open MR-guided injections. **Neurosurg Q** 18:1–6, 2008 [21]).*

Diffusion Tensor Imaging

From the earliest report on the use of DTI to visualize neural pathological conditions (59), it has been clear that this technique has great potential for use in detecting inflammatory brain conditions. It is also proving to be promising for evaluation of stroke, dementia, and diffuse axonal head injury and to aid in surgical navigation in brain tumor resections. It is also being explored for evaluation of myelopathy in the cervical spinal cord. It is very demanding from the point of view of motion suppression, but increasing clinician experience with the special requirements is leading to steady advances in establishing the utility of the technique.

Physical Basis

Nuclear magnetic resonance generally depends on using a radiofrequency stimulation to push energy into a group of nuclei and then using an antenna to detect the decay of the stimulated signal. For a given type of atomic nucleus, such as the single proton nucleus of

hydrogen atoms, there is a nuclear spin rate or frequency that is related to any magnetic field applied to the nucleus according to a physical relationship we call the gyromagnetic ratio. This means that, for instance, in a 4.7-T magnetic field, hydrogen nuclei will be aligned with the direction of the main magnetic field and have a natural spin rate (resonant frequency) of 200 MHz; in a 1.5-T magnet, the spin rate will be 64 MHz, and so on. Therefore, for a given magnet field strength, we know the resonant frequency for hydrogen nuclei and can pump in a pulse of radiofrequency energy at that resonant frequency, thus causing most of the protons in the volume to spin in phase with each other. They will then emit a radiosignal at that frequency that can be detected when the incoming stimulus pulse is turned off. With elapse of time over tens and hundreds of milliseconds, the protons will gradually lose their coherent behavior: Some will spin a little faster and some a little slower, and the return signal will gradually decay away.

When we measure the T1 and T2 decay rates, we are observing the effects of the spins interacting with their surroundings or "matrix." For instance, a little bit of iron in the tissue will perturb the magnetic environment to a variable degree (T1 decay), and we will also see the effects of the protons interacting with each other (spin-spin or T2 decay). Because these decays occur at differing rates in different tissues, we can see contrast between tissues that can be expressed as gray or white in an image of a volume that we are measuring.

In MRI, we use magnetic gradients in 3 planes to assign a slightly different field strength to each location in the tissue volume. For instance, in the very center, the field strength could be 4.7 T, but a little to the right it would be 4.7001 T and a little to the left it would be 4.699 T. The protons on the right now spin at 200.001 MHz, and the protons on the left spin at 199.99 MHz. In this fashion, we can assign a unique field strength and therefore a unique frequency to each voxel (3-D pixel) in our imaging volume, and we can "listen" individually to the decay rate in each individual volume in the tissue. The entire process is done with a mixed complex of frequencies and a Fourier transform is used to sort them all out.

In diffusion imaging, we rely on a special property of axons to establish a source of information from an entirely different cause of spin decay. A pulsed "diffusion" magnetic gradient is applied so that as water molecules diffuse to different locations in a tissue, their spins dephase because a group of water molecules that started out next to each other in a single field strength now find themselves in different field strengths. Thus, they have different spin rates and the spins dephase from each other, resulting in signal decay. Water molecules in some tissues diffuse equally in all directions (isotropic diffusion), but in nerves and nerve tracts, diffusion takes place preferentially along the long axis of the nerve tract (anisotropic diffusion) (Fig. 14). If a magnetic gradient is directed perpendicular to the direction of a nerve or tract, the water diffusing in the nerve will tend to remain in the same strength region of the gradient and will show relatively little decay from diffusion, gradually becoming brighter relative to the tissue around it. However, if the gradient is then oriented parallel to the direction of the nerve, the anisotropically diffusing water molecules will tend to move up and down the gradient more rapidly compared with isotropically diffusing water molecules and so will actually experience a more rapid signal decay, making the nerve tend to go dark relative to other tissues around it.

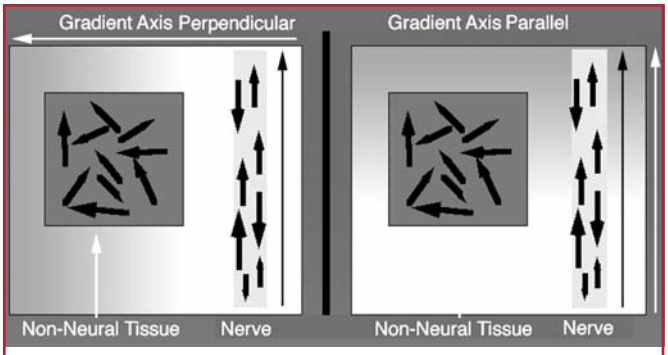

FIGURE 14. *Isotropic and anisotropic diffusion of water molecules in diffusion magnetic resonance imaging. Shades of gray intensity indicate the intensity of the magnetic field, which varies across the image plane because of the imposed pulsed magnetic field gradient. Water diffuses in all directions in most nonneural tissues (isotropically) but diffuses preferentially along the long axis of nerves (anisotropically). When all of the water molecules in a tissue experience identical magnetic field strength despite diffusion movements, the magnetic resonance signal from that tissue remains bright relative to the signal decay in surrounding isotropically diffusing tissue water. This is the situation on the left where the magnetic gradient is oriented perpendicular to the nerve. In the situation on the right, the water molecules in nerve move preferentially to different positions in the gradients more rapidly than in the nonneural tissue so that the signal remains brighter from nonneural tissue.*

However, what happens if the nerve or tract takes a curved course? How do we get the diffusion gradient to be perpendicular or parallel to it? This was the essence of the problem, but the solution comes from very simple mathematical geometry. In essence, if we can determine the degree of anisotropy in each voxel relative to the three principle directional axes, we can provide an estimate of the true dominant direction of anisotropy inside the 3-D space of that voxel. The direction, whether in 2- or 3-D is a vector, however—as will be explained below—we need a more elaborate data structure called a "tensor" in order to fully describe the anisotropy data. Isolated diffusion measurements provide an orientation but not a direction (e.g., the anisotropy goes up and down the z-axis)—it turns out that to fill out the 9 elements of the matrix that describes a tensor in 3-D space we need at least 6 measurements.

In standard DWI, we want to know the total amount of diffusion within a given voxel when viewed with no special attention to direction. For DTI, we want to know both the true magnitude and the true 3-D direction of the anisotropy in each voxel independent of the angle from which we view the voxel. This information is used in 2 different ways. One way is to make an image slice in which the relative amount of anisotropy

is described as the fractional anisotropy (FA), which more or less determines how bright a voxel will be, and uses a standard set of colors to depict some of the information about the orientation of the fiber tracts. This results in cross sections showing some of the information about bulk orientation of white matter tracts in regions of the brain. The other way is for tractography. Here, various mathematical algorithms are applied to generate linear tracts in 3 dimensions that represent the course of bundles of axons in the white matter of the brain or of nerve fibers in peripheral nerves (Fig. 15).

From one point of view, the development of DTI and tractography was hindered for many years by a mathematical model deriving from Basser et al. (6) due to the "elipsoid" formalism that takes a different approach to the analysis than in the original vector and tensor model from Filler (29) and Richards (59) that underlies modern tractography. The equations used for the first tractographic image are as follows:

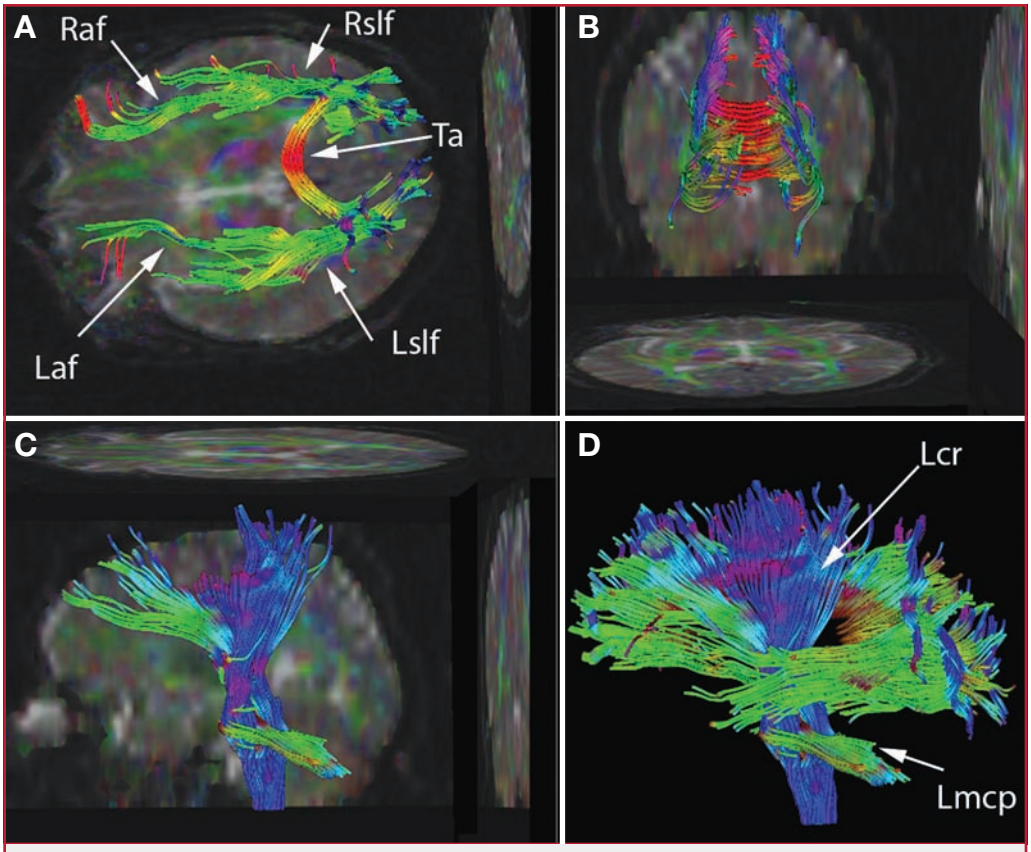

FIGURE 15. *Diffusion tensor imaging data have been used to seed various tractographic assessments of this patient's brain. These are seen in superior (**A**), posterior (**B**), and lateral views (**C** and **D**). The seeds have been used to develop arcuate and superior longitudinal fasciculi in **A** and **B**, for brainstem, and corona radiata in **C** and as combined data sets in **D**. Some of the 2-dimensional projections of the tractographic result are also shown. The data set may be rotated continuously into various planes to better appreciate the structure. Color has been assigned on the basis of the dominant direction of the fibers. There is asymmetry in the tractographic fiber volume between the right (Raf) and left arcuate fasciculus (Laf) (smaller on the left) and between the right (Rslf) and left superior longitudinal fasciculus (Lslf) (smaller on the right). Also seen are tapetum (Ta), left corona radiata (Lcr), and left middle cerebellar peduncle (Lmcp).*

$$(1)\ (\text{Vector length})^2 = BX^2 + BY^2 + BZ^2$$

(2a) Diffusion vector angle between BX and BY = arctan (BY/BX)

(2b) Diffusion vector angle between BX and BZ = arctan (BX/BZ)

(2c) Diffusion vector angle between BY and BZ = arctan (BY/BZ)

The first of these basic equations establish a vector length analogous to what is now called the axial diffusivity (B is an image intensity measure related to the effects of different decay time measured in each of the three axes assessed in three separate measurements, X then Y then Z). This vector length calculation has the important effect of making the measurement of the amount of anisotrophic diffusion in a given voxel independent of the orientation of the anisotropy relative to the orientation of the gradients applied. This made it possible to make, for the first time, a valid image showing the degree of anisotropy in all parts of each image slice. Previously—in a standard diffusion imaging model—a given tract would be bright or dark depending on its orientation in a given voxel even if it was highly anisotropic at that location.

The second set of equations allows us to take three looks at our voxel—each seeing it in 2 dimensions. It uses the arctangent function to measure the angle between the neural tract and the gradient axis direction that is in denominator of the equation. If BY is 0.1 and BX is nearly 1.0, then the arctangent of BY/BX will be about 5 degrees. When the measure is equal in two directions (Y = 0.5 and X = 0.5), the arctangent is 45 degrees.

Because of the vector length and the arctangent function, we can correctly interpret a voxel in which all three angles of measurement are equal. It does not describe a sphere nor does it describe an isotropic voxel. We know it has length and is oriented at 45 degrees to the reference frame—a line along the diagonal of the cube. We can also depict the arctangent value in successive voxels to see coherence in the angle of direction from voxel to voxel as we progress along a neural tract.

Basser and LeBihan (6, 7) proposed that each voxel be viewed as containing an ellipsoid that needed to be defined in shape from 6 different gradient measurements rather than just 3 (55). Although it is true that the thickness of the ellipsoid encodes relevant information about the fine structure inside each voxel, the practical finding has been that only the FA and the primary eigenvector (the length and direction of the long axis of each ellipsoid) has been required for tractography because the tensor model as originally described by Filler, Howe, and Richards models axons. In their fundamental anatomy, these are linear structures and any analysis that turns them into series of complexly shaped and directed ellipsoids can actually obscure the underlying biological and biophysical characteristics. Collecting images that accurately describe the ellipsoids is still a usable formalism but the measurements of the thickness and equatorial orientation of the "jellybean" have so far proven to have little use in tractography. The ellipsoid representation makes more sense in some areas of physics such as magnetic or electric field studies, but has no clear biological correlate in neural tract tracing. Most importantly, if 2 tracts are crossing in a single voxel, the ellipsoid fuses and obscures the axonal data.

As discussed below there is an equally usable formalism that is closer to the anatomy of the axons and neural tracts. In any case, the data processing will continue to advance in complexity as dozens or even hundreds of different gradient axes are sampled—posing significant technical challenge in MRI well into the foreseeable future.

Tensors and Vectors for MRI

At first glance, it might seem that if we measure diffusion in three directions that are the orthogonal x, y, and z axes in a Cartesian 3-D space, then we will be able to know the length and direction of a vector that we can use to support tractography and FA analyses (see Figure 16). The problem is that diffusion measurements in a given orientation do not distinguish which direction the water molecules are moving along the measured axis. In fact, the molecules do move both proximally and distally along the axon, but are only restricted in that that they tend to move along the long axis of the axon rather than freely in any direction.

To understand the implications of this, you can consider a 3-D coordinate system such as we see in Figure 17-I. When we provide a measurement showing diffusivity with resulting intensity of 100 (out of 256) along the x-axis (axial orientation), we must draw this as a line running from +50 to −50. Now we can measure in the y-axis (coronal) and lets use the intensity of 100 again—that is it seems bright in the second axis as well. Returning to our drawing, we draw the line from +50 to −50 on the y-axis.

If we look for an axon line that would meet this description, we get 4 different options on the vectors that might tell us where the axon might be. When we take a third measure—this time in the z-axis (sagittal) and again get a result of a high intensity of 100, we have to draw a third line—this time from +50 to −50 on the z-axis. We now have eight different possible solutions—8 different diagonal vector lines running through each of the 8 octants of 3-D space in our voxel.

We can now start to get some help in figuring out the real tract direction if we measure in a fourth axis and then a fifth axis, each oriented along one of the diagonals as shown in Figure 17-II. When this comes back as a low intensity of 3, we know we can throw out any of the vectors that had no significant apparent length in the 4 octants that our plane passes through. A sixth measurement is then made along one of the remaining diagonals which—in this example—comes back as a low intensity of 4 (see Figure 17-III). This eliminated 2 more octants and leaves only 1 possible solution.

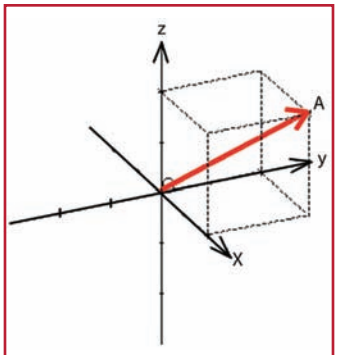

FIGURE 16. *A Cartesian orthogonal frame of reference depicting Vector A. The measurement of the projection of this vector onto each of the three axes, X, Y, and Z is 2 units. Because all of the measurements are positive, the vector (A) points into the octant of space bound on each side by the positive half of each axis.*

If, instead, the sixth measurement had been along the diagonal with the actual neural tract, it would measure out around 140—which happens to follow the Pythagorean theorem relative to our other positive measurements [hypotenuse of a right triangle equals the square root of the of the sum of the squares of the 2 sides: $(100)^2 + (100)^2 = (140)^2$]. With this information, we can be confident that 1 pair of vectors represents the line across our voxel that is the correct source of the signal.

The fact that 6 measurements will always solve the problem seems puzzling, but we can gain confidence by understanding that there is a basis for this in mathematical geometry. The information comes from a special area called tensor analysis.

It is not true that a tensor is just a 3-D vector. Tensors are defined on complex mathematical grounds and do not necessarily have any simple geometric equivalent the physician or biologist can readily rely on to support an understanding of them. Einstein struggled with aspects of tensor theory for a few years before he was able to understand them well enough to use them as the basis for his theory of relativity. To make matters worse, there a number of different ways that tensors can be explained and defined—some deriving from formal modern mathematics, some from physics, some from engineering.

For the purpose of understanding diffusion tensor imaging, however, there is a reasonably accessible approach. A scalar is a simple number. A vector has a length and a direction. A scalar can also be described as a tensor of rank 0. A vector can also be described as a tensor of rank 1.

In the example above, we showed a number of vectors that were bound to the 0 point of a Cartesian coordinate system. It is readily apparent that these vectors were 3-D objects. Each

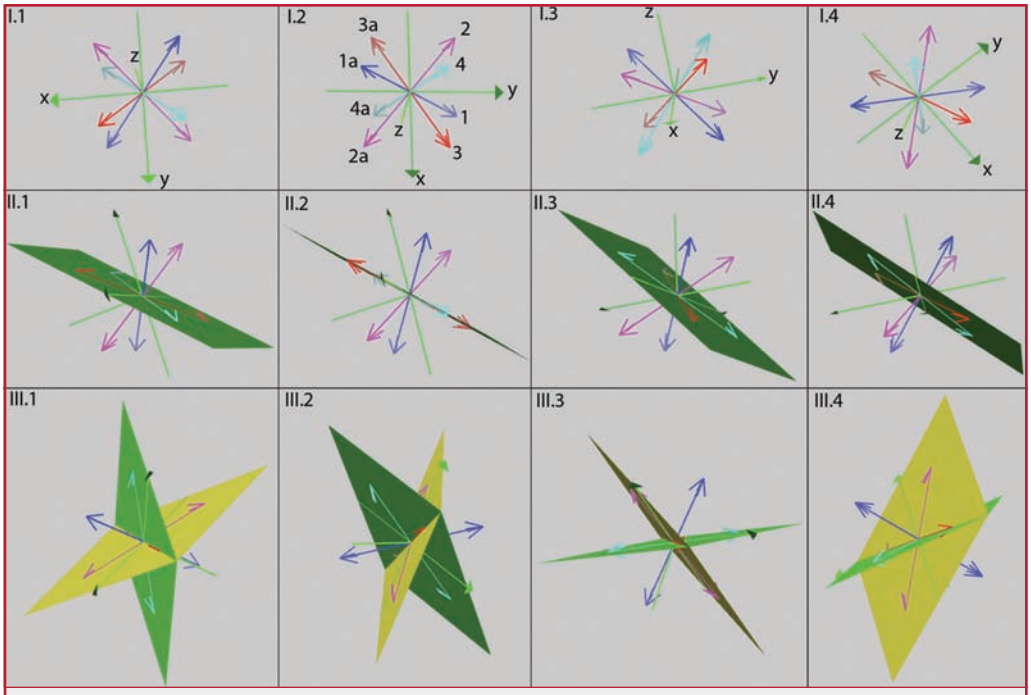

FIGURE 17. *Explanation of antisymmetric dyadic tensor. For each of 3 graph series (I–III) there are 4 different rotations shown to help with visualization. (I) For diffusion measurements along each axis, the direction (sign) is not known. In this example the neural tract is running along the diagonal of the voxel so the measurements on X, Y, and Z are equal. As shown, the ambiguity leads to eight possible vectors (1 and 1a: blue; 2 and 2a: purple; 3 and 3a: red; 4 and 4a: turquoise) along the 4 diagonals of the space. This uncertainty arises when only 3 orthogonal diffusion directions are measured. Each vector runs along a diagonal in 1 of the 8 possible octants of this Cartesian space. We know that 6 of the vectors must be artifactual "ghosts" but we must use 3 more diffusion gradient acquisition directions to distinguish the ghosts from the dyad that actually represents the true neural tract orientation. (II) To clarify the situations, 2 more gradient axes have been measured, each of which was oriented along 1 of the diagonals of the space. A green plane determined by these 2 new measurement lines has been drawn. Notice that this plane incorporates the red (3 and 3a) and the turquoise (4 and 4a) vector pairs. Because our measurement was near 0 in these 2 directions, we can discard the 4 vectors in these 4 octants. (III) A sixth gradient measure has now been made. This also had a very low intensity (rapid decay) we know we can discard the 2 vectors in these 2 octants as well. A yellow plane that incorporates the red (3 and 3a) and the purple (2 and 2a) vectors is shown to demonstrate how the actual vector can have length along all 6 Cartesian axes but not be zeroed by the 2 diagonal planes. Notice that by observing the various rotations, we see that the dyad made up of the blue vectors (1 and 1a) runs in the octants that remain. This shows how 6 measurements can orient the dyad and determine which of 4 possibilities is the true tractographic course.*

vector could be "expanded" for its description. Expansion is a mathematical term that means we could give a scalar on each of the 3 axes and use these 3 numbers to uniquely describe the vector (see figure 16). As we saw in our example, 3 measurements might be enough to describe a vector, but if we don't know the sign or direction on each axis, then this clearly is not enough information to describe the direction of an axon or neural tract as it traverses our MRI voxel.

For tractography, we need to use some kind of tensor of rank 2. There are a number of different mathematical constructs that are rank 2 tensors. One thing they all share in common is that they can be fully described by 9 measurements—often written out in a 3-by-3 matrix. However, since 6 measurements fully describe our neural tract you might expect that there is some special type of tensor we need to focus on.

The correct construct is called a dyad. This is a structure that has a scalar quantity and 2 directions. Fortunately for biologists and physicians, it is acceptable to conceive of a dyad as being made up of 2 vectors. Even more specifically, what we need for our neural tract is a type of dyad called an anti-symmetric dyad. This is a dyad in which the 2 vectors are identical in length (symmetric), but have exactly opposite directions.

One consequence of the anti-symmetry is that we don't need all 9 measurements to fully describe the dyad. Three of the measurements can be dispensed with because of the symmetric nature of the mathematical structure.

Because an antisymmetric dyad is a special case of a tensor of second rank, we can take advantage of a wide expanse of mathematical formulations for assembling and manipulating the data we collect. However, it is not true that our diffusion tensor measurements form a classical tensor field.

One of the original ideas behind tensor math was the problem in physics and engineering that arises when we have a stress applied to a surface of a cube. We consider that the cube is placed under strain and is deformed by the tension of the applied force. However, the strain will differ from place to place in the solid depending on the material it is made of and the way that the force of the stress is being applied. A tensor field might be used to generate force vectors for each unit volume of the cube in a predictable mathematical progression.

However in the diffusion tensor data set in clinical MRI, the field of tensors in the brain (for instance) is determined by anatomy and really cannot be arrived at by any complex mathematical formula. We can generate tractographic atlas data to use in algorithms to help guide the tractographic process, however, for the most part, the preference has been to allow the tractographic process to proceed from the data collected for each voxel in the imaged area.

Tractography is done in a wide variety of ways, but there are 2 main classes of approaches to the problem. In 1 group of

methods, we more or less follow from 1 dyadic line to the next using various seeds as starting points. In the other group of methods we lay out the field of dyadic tensor lines and try to allow a line to find the lowest energy course (the path of least resistance) through the thicket of dyads.

Future Challenges

An additional challenge for tractography derives from the fact that diffusion imaging in general and diffusion tensor imaging especially, are extremely sensitive to motion. This is because we are trying to measure the motion of water molecules due to diffusion. At a very fine level, brain pulsations due to the arterial pulse and respiratory effects on the venous pressure—along with bulk movements from respiration, can only be suppressed by extraordinarily rapid imaging—images requiring a fraction of a second to acquire.

Even with complete suppression of motion, brain tractography is limited by the problem of fiber tracts in differing directions passing through each other. Many of these conflicts can be resolved with increasingly fine spatial resolution, so that a given voxel tends to contain fascicles mostly with a single direction. However, very fine spatial resolution requires very high signal to noise performance. This can be accomplished with long repetitive scans in high field magnets (3-T), but the very fast echo planar scans used to suppress motion and acquire multiple gradient axes tend to lose ground on signal strength and spatial resolution. Abandoning the ellipsoid, we can use multiple vectors or higher order tensors to allow multiple axonal directions in a single voxel.

There are a few situations in which a limited number of gradient orientations can be sufficient. This is the case if we use an Atlas or a non-diffusion nerve image in peripheral nerve tractography as a guide to make decisions about which axes to accept and which to ignore. Another simple method proposed by Kinosada (47, 48) is to use 1 or 2 gradient acquisitions to generate bright spots in cross sectional images. We then apply maximum intensity projection methods to look through a stack of these images in order to convert the 2-D data to 3-D tractographic images, much like the methodology is some forms of MR angiography. This is more likely to be effective with peripheral nerve since it has low resolving power for diverging tracts along complex courses such as we find more frequently in the brain.

In any case, the compromise of using the single primary eigenvector or the equivalent anti-symmetric dyad and dispensing with full use of the additional information in the ellipsoid, has made it possible to carry out good tractography in 1.5-T MRI scanners on most patients. The power of DTI is therefore now starting to be revealed.

Clinical Utility of DTI

A critical aspect to keep in mind is that in T2 MRN, the nerve anatomy becomes progressively more clear and detailed as the pathological condition becomes more severe. The opposite is true of DTI. Any significant irritative or ischemic abnormality tends to decrease the anisotropy and therefore to make the involved neural tracts disappear. Alhough this means that DTI tractography studies can be read for tract "drop out" as a sign of a pathological condition, it also means that results must be assessed very carefully when they are relied on to demarcate tract borders near tumors or other irritative lesions.

Although simple DWI is very useful for identifying cerebral infarctions, DTI has greatly expanded the clinical utility of diffusion decay information. The key difference between DWI and DTI is reliance on the apparent diffusion coefficient (ADC) in DWI versus the FA in DTI. Simply put, the ADC provides a single "scalar" number that estimates the relative degree of anisotropy versus isotropy in a given voxel. The estimate is flawed because it eliminates the anisotropy signal arising from differences in orientation of the direction of diffusion that occur between the axons in the volume and the arbitrarily chosen imaging planes. Conversely, the FA measures the anisotropy in each voxel in a way that closely approximates the true length of the principal vector in each voxel, whatever direction it is pointing in.

The beneficial effect on the quality of diffusion data that results from use of FA as opposed to ADC is already clear from the first few formal outcome studies that evaluated the clinical utility of the FA measurement. In a study of 17 patients comparing ADC and FA measurements in white matter tracts adjacent to spontaneous intracerebral hemorrhage (63), the FA provided a statistically significant prediction of outcome, whereas ADC did not. In a longitudinal study with repeat imaging and FA analysis in 23 patients with traumatic brain injury (60), the increase in FA was highly correlated with an increase in Glasgow outcome score during recovery and most of this correlation derived from the principal eigenvalue parallel to the main direction of the axons in a given voxel.

The use of tractography in image segmentation for tumor resection planning has now also been formally evaluated in a randomized, controlled, prospective trial (62) involving 238 patients that compared success of gross total resection, Karnofsky performance at 6 months, and survival from high-grade gliomas using neuronavigation guidance from DTI tractography versus neuronavigation from standard MRI. This study showed statistically significant improvement in these measures when DTI tractography was used, resulting in a 43% reduction in risk of death in the hazard risk time period evaluated.

CONCLUSIONS

At this point, it is clear that when the precise location of a peripheral nerve lesion cannot be determined externally, nerve imaging should be performed. Because MRN demonstrates pathological lesions as well as anatomy because of its view into the intrinsic signal from the endoneurial fluid, it should be the method of choice unless there is some overwhelming reason to not want to know the available information.

DTI provides increased sensitivity for CNS pathological conditions relative to other magnetic resonance-based imaging techniques. Because FA encodes directional and functional information not captured by other techniques, its information content regarding pathological conditions affecting both structure and membrane stability is higher. It seems to be indicated

for diagnostic and prognostic information as well as for tracking recovery in the setting of ischemic, traumatic, inflammatory, infectious, and degenerative disease, particularly when an asymmetric pathological condition that will allow comparison between an ipsilateral affected side and contralateral unaffected side is suspected.

As with spine imaging, neurographic and tractographic imaging can provide false-positive findings. However, these are often very specific anatomically and can be considered and tested for clinical relevance.

The technical aspects of imaging hardware that will improve MRN in the future include larger areas of excellent magnetic field homogeneity, which will allow for large field-of-view studies with uniform fat suppression and image quality throughout the larger image volumes, and improvements in antenna coil technology, which will also tend to improve the signal-to-noise ratio. Use of black blood contrast agents such as ferrite agents could improve visualization of very small nerves for which the anatomic distinction from very small vessels is unreliable.

For diffusion-based methods such as DTI, even the vibration of the scanner caused by the interactions between the gradient coils and the main magnetic field have become a significant problem, limiting spatial resolution. This is the interaction that causes the typical knocking sound, which can rise to a deafening level when high fields, powerful, fast-rising gradients, and very rapid pulse sequences are deployed. The solutions here include design of magnets with inertially resistant gradient coils that provide physical dampening of vibration along with advances in the design of balancing gradients that cancel the physical and mechanical effects of the magnetic interaction. The resulting improvement in spatial resolution and signal strength will be necessary to help to resolve brain regions in which fiber bundles pass through each other in different directions or in which they diverge slowly.

The introduction of imaging techniques capable of demonstrating the intrinsic signal of nerves as well as of preserving and displaying structural linear properties of neural tissue in general is progressively transforming all neuroimaging as these techniques transform our approach to diagnosis, treatment planning, and surgical access. The next 10 years will be an extremely exciting period for the various forms of neural tractography. It is reasonable to expect that there will be a logarithmic expansion of the use of these techniques so that more than 5 million such imaging studies will probably be performed in the next 10 years. Many of the fundamental obstacles have been overcome and advances in the power of imaging equipment and postprocessing technology will similarly help drive these methods to the forefront of neurology and neurosurgery.

REFERENCES

1. Aagaard BD, Maravilla KR, Kliot M: MR neurography. MR imaging of peripheral nerves. **Magn Res Imaging Clin N Am** 6:179–194, 1998.
2. Aagaard BD, Maravilla KR, Kliot M: Magnetic resonance neurography: Magnetic resonance imaging of peripheral nerves. **Neuroimaging Clin N Am** 11:viii, 131–146, 2001.
3. Ambrose J, Hounsfield G: Computerized transverse axial tomography. **Br J Radiol** 46:148–149, 1973.
4. Atlas SW: *Magnetic Resonance Imaging of the Brain and Spine.* New York, Raven Press, 1996.
5. Basser PJ, LeBihan D: Fiber orientation mapping in an anisotropic medium with NMR diffusion spectroscopy. Presented at the 11th Annual Meeting of the Society for Magnetic Resonance in Medicine, Berlin, Germany, August 8–14, 1992.
6. Basser PJ, Mattiello J, LeBihan D: MR diffusion tensor spectroscopy and imaging. **Biophys J** 66:259–267, 1994.
7. Basser PJ, Mattielo J, LeBihan D: Diagonal and off-diagonal components of the self-diffusion tensor: Their relation to and estimation from the NMR spin-echo signal. Presented at the 11th Annual Meeting of the Society for Magnetic Resonance in Medicine, Berlin, Germany, August 8–14, 1992.
8. Bowen BC, Pattany PM, Saraf-Lavi E, Maravilla KR: The brachial plexus: Normal anatomy, pathology, and MR imaging. **Neuroimaging Clin N Am** 14:59–85, vii–viii, 2004.
9. Chappell KE, Robson MD, Stonebridge-Foster A, Glover A, Allsop JM, Williams AD, Herlihy AH, Moss J, Gishen P, Bydder GM: Magic angle effects in MR neurography. **AJNR Am J Neuroradiol** 25:431–440, 2004.
10. Chua TC, Wen W, Slavin MJ, Sachdev PS: Diffusion tensor imaging in mild cognitive impairment and Alzheimer's disease: A review. **Curr Opin Neurol** 21:83–92, 2008.
11. Dailey AT, Tsuruda JS, Filler AG, Maravilla KR, Goodkin R, Kliot M: Magnetic resonance neurography of peripheral nerve degeneration and regeneration. **Lancet** 350:1221–1222, 1997.
12. Deacon TW: Cortical connections of the inferior arcuate sulcus cortex in the macaque brain. **Brain Res** 573:8–26, 1992.
13. Deacon TW: *The Symbolic Species: The Co-evolution of Language and the Brain.* New York, WW Norton, 1997.
14. Diehl B, Busch RM, Duncan JS, Piao Z, Tkach J, Lders HO: Abnormalities in diffusion tensor imaging of the uncinate fasciculus relate to reduced memory in temporal lobe epilepsy. **Epilepsia** 49:1409–1418, 2008.
15. Filler AG: Anatomical specializations in the hominoid lumbar region. **Am J Phys Anthropol** 54:218, 1981.
16. Filler AG: Axonal transport and MR imaging: Prospects for contrast agent development. **J Magn Reson Imaging** 4:259–267, 1994.
17. Filler AG: *Axial Character Seriation in Mammals: An Historical and Morphological Exploration of the Origin, Development, Use and Current Collapse of the Homology Paradigm.* Boca Raton, BrownWalker Press, 2007.
18. Filler AG: Homeotic evolution in the mammalia: Diversification of therian axial seriation and the morphogenetic basis of human origins. **PLoS ONE** 2:e1019, 2007.
19. Filler AG: The emergence and optimization of upright posture among hominiform hominoids and the evolutionary pathophysiology of back pain. **Neurosurg Focus** 23:E4, 2007.
20. Filler AG: Piriformis and related entrapment syndromes: Diagnosis & management. **Neurosurg Clin N Am** 19:609–622, vii; 2008.
21. Filler AG: Diagnosis and management of pudendal nerve entrapment syndromes: Impact of MR neurography and open MR-guided injections. **Neurosurg Q** 18:1–6, 2008.
22. Filler AG, Bell BA: Axonal transport, imaging, and the diagnosis of nerve compression. **Br J Neurosurg** 6:293–295, 1992.
23. Filler AG, Haynes J, Jordan SE, Prager J, Villablanca JP, Farahani K, McBride DQ, Tsuruda JS, Morisoli B, Batzdorf U, Johnson JP: Sciatica of nondisc origin and piriformis syndrome: Diagnosis by magnetic resonance neurography and interventional magnetic resonance imaging with outcome study of resulting treatment. **J Neurosurg Spine** 2:99–115, 2005.
24. Filler AG, Howe, FA: Images, apparatus, algorithms, and methods. GB 9205541. UK Patent Office. 1992.
25. Filler AG, Howe FA, Hayes CE, Kliot M, Winn HR, Bell BA, Griffiths JR, Tsuruda JS: Magnetic resonance neurography. **Lancet** 341:659–661, 1993.
26. Filler AG, Howe FA, Richards TL, Tsuruda JS: Image neurography and diffusion anisotropy imaging. In, World Intellectual Property Organization IB (ed), 1993.
27. Filler AG, Kliot M, Howe FA, Hayes CE, Saunders DE, Goodkin R, Bell BA, Winn HR, Griffiths JR, Tsuruda JS: Application of magnetic resonance neurography in the evaluation of patients with peripheral nerve pathology. **J Neurosurg** 85:299–309, 1996.
28. Filler AG, Maravilla KR, Tsuruda JS: MR neurography and muscle MR imaging for image diagnosis of disorders affecting the peripheral nerves and musculature. **Neurol Clin** 22:643–682, vi-vii, 2004.

29. Filler AG, Tsuruda JS, Richards TL, Howe FA: Images, apparatus, algorithms, and methods. GB 9216383. UK Patent Office. 1992.
30. Filler AG, Tsuruda JS, Richards TL, Howe FA: Image neurography and diffusion anisotropy imaging. US patent 5,560,360. Filed March 8, 1993; granted October 1, 1996.
31. Filler AG, Whiteside G, Bacon M, Frederickson M, Howe FA, Rabinowitz MK, Sokoloff AJ, Deacon TW, Abell C, Munglani R, Griffiths JR, Bell BA, Lever AM: Successful use of axonal transport for drug delivery by synthetic molecular vehicles. **Nat Preced** 2008. http://hdl.handle.net/10101/npre.2008.2164.1. Accessed August 6, 2008.
32. Filler AG, Winn HR, Howe FA, Griffiths JR, Bell BA, Deacon TW: Axonal transport of superparamagnetic metal oxide particles: Potential for magnetic resonance assessments of axoplasmic flow in clinical neuroscience. Presented at 10th Annual Meeting of the Society for Magnetic Resonance in Medicine, San Francisco, California, 1991.
33. Filler AG, Winn HR, Westrum LE, Sirrotta P, Krohn K, Deacon TW: Intramuscular injection of WGA yields systemic distribution adequate for imaging of axonal transport in intact animals. **Soc Neurosci Abs** 17:1480, 1991.
34. Grant GA, Britz GW, Goodkin R, Jarvik JG, Maravilla K, Kliot M: The utility of magnetic resonance imaging in evaluating peripheral nerve disorders. **Muscle Nerve** 25:314–331, 2002.
35. Grant GA, Goodkin R, Maravilla KR, Kliot M: MR neurography: Diagnostic utility in the surgical treatment of peripheral nerve disorders. **Neuroimaging Clin N Am** 14:115–133, 2004.
36. Heide AC, Richards TL, Alvord EC Jr, Peterson J, Rose LM: Diffusion imaging of experimental allergic encephalomyelitis. **Magn Reson Med** 29:478–484, 1993.
37. Hounsfield GN: Computerized transverse axial scanning (tomography). 1. Description of the system. **Br J Radiol** 46:1016–1022, 1973.
38. Howe FA, Filler AG, Bell BA, Griffiths JR: Magnetic resonance neurography. **Magn Reson Med** 28:328–338, 1992.
39. Howe FA, Filler AG, Bell BA, Griffiths JR: Magnetic resonance neurography: Optimizing imaging techniques for peripheral nerve identification. Presented at the 11th Annual Meeting of the Society for Magnetic Resonance in Medicine, Berlin, Germany, August 8–14, 1992.
40. Igarashi T, Yabuki S, Kikuchi S, Myers RR: Effect of acute nerve root compression on endoneurial fluid pressure and blood flow in rat dorsal root ganglia. **J Orthop Res** 23:420–424, 2005.
41. Jarvik JG, Comstock BA, Heagerty PJ, Haynor DR, Fulton-Kehoe D, Kliot M, Franklin GM: Magnetic resonance imaging compared with electrodiagnostic studies in patients with suspected carpal tunnel syndrome: Predicting symptoms, function, and surgical benefit at 1 year. **J Neurosurg** 108:541–550, 2008.
42. Jarvik JG, Yuen E, Haynor DR, Bradley CM, Fulton-Kehoe D, Smith-Weller T, Wu R, Kliot M, Kraft G, Wang L, Erlich V, Heagerty PJ, Franklin GM: MR nerve imaging in a prospective cohort of patients with suspected carpal tunnel syndrome. **Neurology** 58:1597–1602, 2002.
43. Kakuda W, Lansberg MG, Thijs VN, Kemp SM, Bammer R, Wechsler LR, Moseley ME, Parks MP, Albers GW: Optimal definition for PWI/DWI mismatch in acute ischemic stroke patients. **J Cereb Blood Flow Metab** 28: 887–891, 2008.
44. Kent DL, Haynor DR, Longstreth WT, Jr., Larson EB: American College of Physicians, Position paper: Magnetic resonance imaging of brain and spine: A revised statement. **Ann Intern Med** 120:872–875, 1994.
45. Kent DL, Haynor DR, Longstreth WT Jr, Larson EB: The clinical efficacy of magnetic resonance imaging in neuroimaging. **Ann Intern Med** 120:856–871, 1994.
46. Khalil C, Hancart C, Le Thuc V, Chantelot C, Chechin D, Cotten A: Diffusion tensor imaging and tractography of the median nerve in carpal tunnel syndrome: Preliminary results. **Eur Radiol** 18:2283-2291, 2008.
47. Kinosada Y, Nakagawa T: New non-invasive technique to visualize three-dimensional anatomic structures of myelinated white matter tracts of human brain in vivo. **Front Med Biol Eng** 6:37–49, 1994.
48. Kinosada Y, Ono M, Okuda Y, Seta H, Hada Y, Hattori T, Nomura Y, Sakuma H, Takeda K, Ishii Y: MR tractography—visualization of structure of nerve fiber system from diffusion weighted images with maximum intensity projection method (in Japanese). **Nippon Igaku Hoshasen Gakkai Zasshi** 53:171–179, 1993.
49. Kramer M, Deacon TW, Sokoloff A, Filler A: Organization of motorneurons innervating epaxial and hypaxial musculature in the frog, rat, and monkey. **Soc Neurosci Abstr** 13:526, 1987.
50. Kuntz CT, Blake L, Britz G, Filler A, Hayes CE, Goodkin R, Tsuruda J, Maravilla K, Kliot M: Magnetic resonance neurography of peripheral nerve lesions in the lower extremity. **Neurosurgery** 39:750–757, 1996.
51. Lansberg MG, Thijs VN, O'Brien MW, Ali JO, de Crespigny AJ, Tong DC, Moseley ME, Albers GW: Evolution of apparent diffusion coefficient, diffusion-weighted, and T2-weighted signal intensity of acute stroke. **AJNR Am J Neuroradiol** 22:637–644, 2001.
52. Le Bihan D: Molecular diffusion nuclear magnetic resonance imaging. **Magn Reson Q** 7:1–30, 1991.
53. LeBihan D: IVIM method measures diffusion and perfusion. **Diagn Imaging** 12:133, 136, 1990.
54. Mizisin AP, Kalichman MW, Myers RR, Powell HC: Role of the blood-nerve barrier in experimental nerve edema. **Toxicol Pathol** 18:170–185, 1990.
55. Mori S: *Introduction to Diffusion Tensor Imaging*. New York, Elsevier, 2007.
56. Moseley ME, Kucharczyk J, Mintorovitch J, Cohen Y, Kurhanewicz J, Derugin N, Asgari H, Norman D: Diffusion-weighted MR imaging of acute stroke: Correlation with T2-weighted and magnetic susceptibility-enhanced MR imaging in cats. **AJNR Am J Radiol** 11:423–429, 1990.
57. Myers RR, Rydevik BL, Heckman HM, Powell HC: Proximodistal gradient in endoneurial fluid pressure. **Exp Neurol** 102:368–370, 1988.
58. Poduslo JF, Low PA, Nickander KK, Dyck PJ: Mammalian endoneurial fluid: Collection and protein analysis from normal and crushed nerves. **Brain Res** 332:91–102, 1985.
59. Richards TL, Heide AC, Tsuruda JS, Alvord EC: Vector analysis of diffusion images in experimental allergic encephalomyelitis. Presented at the 11th Annual Meeting of the Society for Magnetic Resonance in Medicine, Berlin, Germany, August 8–14, 1992.
60. Sidaros A, Engberg AW, Sidaros K, Liptrot MG, Herning M, Petersen P, Paulson OB, Jernigan TL, Rostrup E: Diffusion tensor imaging during recovery from severe traumatic brain injury and relation to clinical outcome: A longitudinal study. **Brain** 131:559–572, 2008.
61. Viallon M, Vargas MI, Jlassi H, Lövblad KO, Delavelle J: High-resolution and functional magnetic resonance imaging of the brachial plexus using an isotropic 3D T2 STIR (short term inversion recovery) SPACE sequence and diffusion tensor imaging. **Eur Radiol** 18:1018–1023, 2008.
62. Wu JS, Zhou LF, Tang WJ, Mao Y, Hu J, Song YY, Hong XN, Du GH: Clinical evaluation and follow-up outcome of diffusion tensor imaging-based functional neuronavigation: A prospective, controlled study in patients with gliomas involving pyramidal tracts. **Neurosurgery** 61:935–949, 2007.
63. Yoshioka H, Horikoshi T, Aoki S, Hori M, Ishigame K, Uchida M, Sugita M, Araki T, Kinouchi H: Diffusion tensor tractography predicts motor functional outcome in patients with spontaneous intracerebral hemorrhage. **Neurosurgery** 62:97–103, 2008.

Acknowledgments

I thank David Kline, M.D., H. Richard Winn, M.D., B. Anthony Bell, M.D., John Griffiths, D.Phil., Franklyn Howe, D.Phil., Todd Richards, Ph.D., Ken Maravilla, M.D., Terrence Deacon, Ph.D., Jodean Peterson, B.A., and Shirlee Jackson, B.A., for their assistance, contributions, and inspiration in the course of this effort.

Disclosures

Portions of this work were supported by National Institutes of Health Grant PHS 5 T32 GM07117-09 0011 (Harvard University), National Institutes of Health Grant NSTG 5T32 NS-07144-09 (University of Washington), The Wellcome Trust "MR Imaging of Neural Tracts," the UK Cancer Research Campaign, and the Neurosciences Research Foundation of Atkinson Morley's Hospital. Aaron G. Filler, M.D., Ph.D., is a coinventor on patents that cover the use of magnetic resonance neurography and diffusion tensor imaging. He has received funding from the National Institutes of Health, The Wellcome Trust, and the Atkinson Morley's Research Foundation for scientific research related to the subject matter. His clinical neurosurgical practice uses these imaging techniques. He performs radiology interpretations on magnetic resonance neurography and diffusion tensor images. He is a shareholder in NeuroGrafix, a company that administers patent technology licenses under agreement from the University of Washington, which owns the patent and which also manages image data transport for neural tract imaging, although he has not received any funds from NeuroGrafix.